The Report committee for Benjamin B. Weaver

Certifies that this is the approved version of the following report:

Synthesis, Characterization and Magnetic Properties of

$A_xB_{1-x}V_2O_4$ Spinels for A, B = Mg, Co, Zn, Fe, Mn

APPROVED BY

SUPERVISING COMMITTEE:

Supervisor: _____

Yuebing Zheng

Co-Supervisor: _____

Jianshi Zhou

Synthesis, Characterization and Magnetic Properties of

$A_xB_{1-x}V_2O_4$ Spinels for $A, B = Mg, Co, Zn, Fe, Mn$

by

Benjamin B. Weaver, B.S.; M.A.

Presented to the Faculty of the Graduate School

of the University of Texas at Austin

in Partial Fulfillment

of the Requirements

for the Degree of

Master of Science in Engineering

The University of Texas at Austin

August, 2015

Dedicated to Ciara.

Synthesis, Characterization and Magnetic Properties of

$\mathbf{A_xB_{1-x}V_2O_4}$ Spinels for $\mathbf{A, B = Mg, Co, Zn, Fe, Mn}$

by

Benjamin B. Weaver, M.S.E.

The University of Texas at Austin, 2015

SUPERVISORS: Yuebing Zheng, Jianshi Zhou

Report

This work demonstrates the novel synthesis of solid solutions of vanadium spinels A_x B_{1-x} V_2 O_4, where A, B = Mg, Co, Zn, Fe, Mn, and x = $0, 0.25, 0.5, 0.75, 1$. Seventeen samples are synthesized using a microwave-assisted solvothermal (MW-ST) process and annealed in an Ar atmosphere. Materials characterization of samples is carried out by x-ray diffraction (XRD) and inductively coupled plasma (ICP). Magnetic properties of samples are measured by a vibrating sample magnetometer (VSM).

Contents

1 Introduction

Motivation for this project comes from an interest in understanding electronic transitions in vanadium oxides. Reports have demonstrated the localized-to-itinerant electron transition in certain perovskite oxides and spinel oxides under high pressure, with particular interest recently in vanadium oxides. [2], [9], [13] Due to the lattice environment of certain vanadium oxides, orbitals of neighboring vanadium sites can overlap. As the distance between neighboring vanadium sites decreases, the overlap integral increases and at a critical V-V distance, valence electrons undergo a transition from being localized on the vanadium ion to an itinerant state. At ambient pressure, the V-V separation in vanadium oxides is larger than the critical distance and electrons remain localized. But, as pressure is applied to a sample and as the unit cell decreases, the V-V separation can be made to pass through this critical distance, whereupon the electron undergoes a transition to an itinerant state.

Figure 1 shows the evolution of the Néel temperature as a function of inverse V-V bond length. According to this figure, as pressure is increased, the Néel temperature drops off sharply to zero before the critical V-V separation is reached. [2] This corresponds to a transitional region (Region II in the figure) over which the model describing localized electrons breaks down. Understanding the nature of this transition is the motivation for this work

The purpose of this report is to serve as a first step in studying this electronic transition with a larger and more comprehensive set of samples than is found at

present in the literature. We will accomplish this by synthesizing a set of samples whose A-site cation varies in radius, effectively modulating the V-V separation within the unit cell. The A-site cations used in this study are A = Mg, Co, Zn, Fe, Mn. IR effective ionic radii of these ions in the 2+ oxidation state and IV-coordinated environment are 0.57Å, 0.58Å, 0.60Å, 0.63Å, and 0.66Å, respectively. [14]

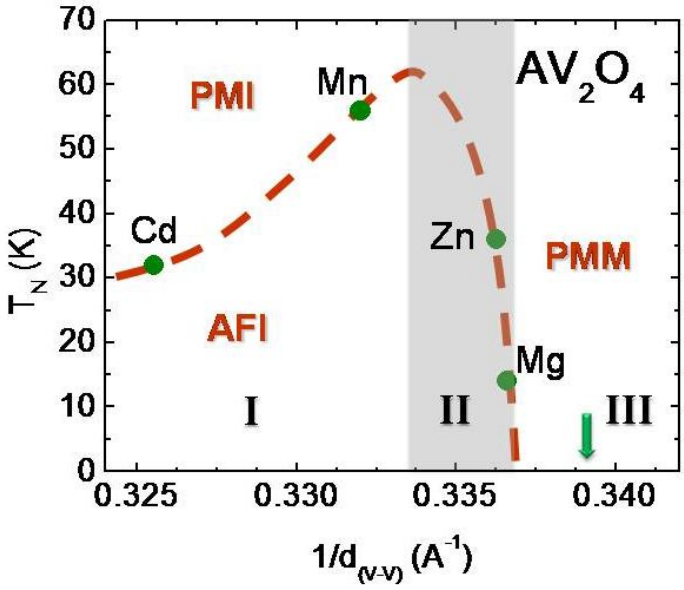

Figure 1: Magnetic phase diagram of AV_2O_4 system with A = Mg, Zn, Mn, Cd. The dashed line shows the expected evolution of the Néel temperature as a function of inverse V-V bond length. The green vertical arrow represents the expected critical distance for localized-to-itinerant electron transition. The original publication of this figure is found in [2].

The full series of $A_xB_{1-x}V_2O_4$ samples include four systems of solid solutions, consisting of Mg-Co, Co-Zn, Zn-Fe, and Fe-Mn systems. Substitutions were incremented so that x = $0, 0.25, 0.5, 0.75, 1$ to generate a total of seventeen samples. This series was chosen to complement the existing body of work that demonstrates synthesis of AV_2O_4 spinels as well as certain of the solid solutions. A comprehensive series such

as this report demonstrates, however, has not previously been reported.

In section 2 we describe the experiment, detailing the synthesis method and sintering process, and characterization of our samples. In section 3, we will analyze the results of this experiment and the significance of these results. Finally, we will end with conclusions in section 4.

2 Experimental details

In this section, we will discuss sample preparation, sample characterization and measurement of their magnetic properties.

2.1 Synthesis

Samples of $A_xB_{1-x}V_2O_4$ were prepared by a two-step process of synthesis and post-heat treatment. Stoichiometric amounts of the appropriate divalent acetate hydrates of Mg, Co, Zn, and Mn or anhydrous acetate of Fe were added to a 30mL glass microwave vial and stirred with a magnetic stir bar in 10mL tetraethylene glycol (TEG) until the acetate was dissolved. In some cases, moderate heat was applied to this mixture to accelerate dissolution. When acetate dissolution reached saturation, a stoichiometric amount of vanadium tri-isopropoxide was added and immediately inserted into an Anton Paar Monowave 300 microwave synthesis reactor, whereupon it was heated as fast as possible to 300°C and irradiated for 30min. Upon cooling, the dark powder precipitate was washed in acetone, sonicated and centrifuged until decanted acetone was clear. The precipitate was air dried in a 100°C oven and ground in a mortar.

Each sample was then annealed in a ceramic tube oven under a steady flow of argon for 6-12 hours at a temperature just below the decomposition of the sample into multiple phases. This decomposition temperature was determined for each sample by heating the sample at a range of temperatures, either increasing the firing

temperature until decomposition began or decreasing temperature until single phase was reached. In this way, the annealing temperature of each sample was optimized to maximize crystallinity, as measured by the sharpness of the XRD pattern, without compromising its single phase character.

2.2 Materials characterization

Samples were characterized using X-ray diffraction (XRD) to determine the crystal structure. XRD patterns were collected on a Rigaku Ultima IV XRD instrument. Chemical composition was determined by inductively coupled plasma atomic emission spectroscopy (ICP-AES) and analysis was carried out with a Varian 715-ES ICP optical emission spectrometer.

2.2.1 X-Ray Diffraction

X-ray diffraction (XRD) was used to determine the purity of sample phases and as a measure of the crystallinity of these samples. XRD patterns were taken of the as-synthesized powder samples after microwave-assisted synthesis and after annealing at higher temperatures. XRD patterns of each sample were analyzed to determine the temperature at which the sample became multiple phase. This typically occurred when the A-site component was reduced to metal. Samples that contained Co were annealed at a temperature no higher than 500^{o}C, the temperature at which Co^{3+} reduced to Co metal in these samples. Samples that contained Fe were annealed a

temperature no higher than 640°C, the temperature at which Fe^{3+} reduced to Fe metal.

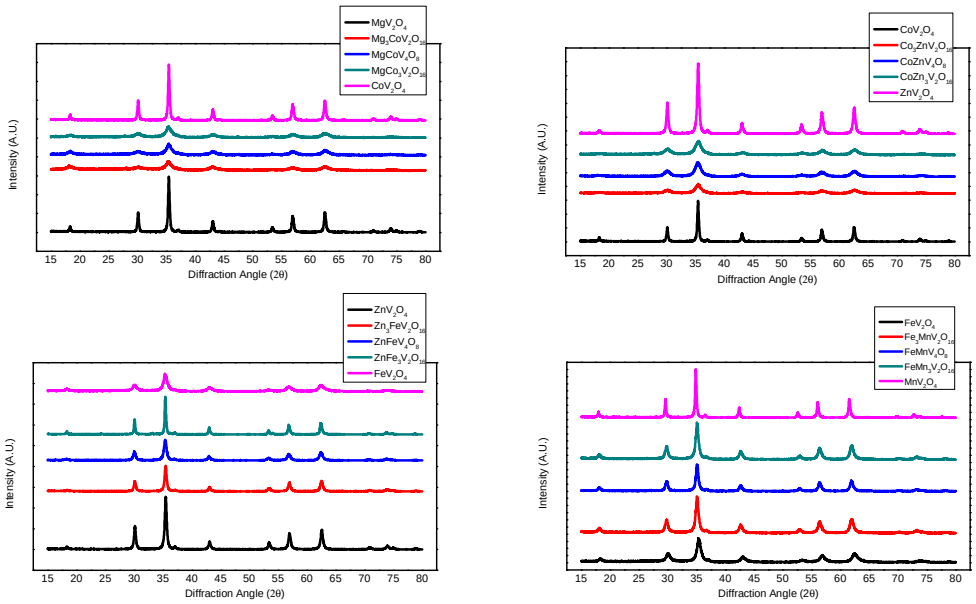

Figure 2: X-ray diffraction patterns for Mg-Co system, Co-Zn system, Zn-Fe system, and Fe-Mn system after annealing in Ar atmosphere.

2.2.2 Inductively Coupled Plasma Atomic Emission Spectroscopy

Inductively coupled plasma atomic emission spectroscopy (ICP-AES) was used to determine the elemental composition of samples by comparing the ratio of vanadium ions to A-site cations. Samples for ICP-AES analysis were prepared by partially dissolving approximately 2mg of powder sample in a solution of 500μL hydrochloric acid and 250μL nitric acid. To this solution, sulfuric acid was added and the vial cap was sealed until the sample was fully dissolved. When dissolution was complete, de-ionized (DI) water was added to make a sample volume of 250μL. A set of three

ICP standards were prepared that included known concentrations of Mg, Co, Zn, Fe, Mn, and V and by comparison to this standard, the stoichiometry of each sample was determined.

In table 1, the nominal and experimental stoichiometries of each sample are presented. Deviations from nominal stoichiometry are largest for Co-containing samples.

A_x	B_{1-x}	$2A_x/V$	$2B_{1-x}/V$
Mg		1.03	
$Mg_{0.75}$	$Co_{0.25}$	0.78	0.28
$Mg_{0.5}$	$Co_{0.5}$	0.51	0.56
$Mg_{0.25}$	$Co_{0.75}$	0.25	0.85
Co		1.12	
$Co_{0.75}$	$Zn_{0.25}$	0.85	0.27
$Co_{0.5}$	$Zn_{0.5}$	0.55	0.53
$Co_{0.25}$	$Zn_{0.75}$	0.29	0.83
Zn		0.97	
$Zn_{0.75}$	$Fe_{0.25}$	0.78	0.25
$Zn_{0.5}$	$Fe_{0.5}$	0.53	0.49
$Zn_{0.25}$	$Fe_{0.75}$	0.73	0.26
Fe		0.97	
$Fe_{0.75}$	$Mn_{0.25}$	0.75	0.26
$Fe_{0.5}$	$Mn_{0.5}$	0.5	0.49
$Fe_{0.25}$	$Mn_{0.75}$	0.78	0.25
Mn		1.03	

Table 1: Chemical composition of $A_xB_{1-x}V_2O_4$ samples as measured by inductively coupled plasma atomic emission spectroscopy. The first and second column are nominal amounts of each element per formula unit in the A-site. The third and fourth columns show the relative amounts of each element per formula unit in the A-site, expressed as a ratio of A-site cation to vanadium ion.

2.3 Measurements of magnetic properties

Magnetic moment measurements were carried out on a vibrating sample magnetometer (VSM), a feature on the physical property measurement system (PPMS) by Quan-

tum Design. Measurements were taken of the magnetic moment as a function of temperature, from 3K to 300K, with an applied field of 100Oe. Both a field cooled (FC) sweep and a zero-field cooled (ZFC) sweep were performed. Magnetic moment was also measured as a function of magnetic field from -1000Oe to 1000Oe, while held at 3K. The temperature dependence of the susceptibility allows us to determine the Curie temperature for specimens that exhibit Curie-Weiss behavior, while the hysteresis loop allows us to determine coercivity.

3 Results and analysis

Conventional solid-state synthesis of AV_2O_4 samples is usually performed under vacuum, requiring evacuated quartz tubes, lengthy reaction times, and repeated grindings to produce quality samples. [3], [6], [1], The method used in this report significantly reduces reaction times and decreases overall sample preparation times.

To demonstrate the usefulness of the microwave-assisted solvothermal method, attempts were made to reproduce $A_xB_{1-x}V_2O_4$ samples under solid state synthesis temperatures similar to temperatures used in post-heat treatments in this report. Reactions of V_2O_3 and appropriate A-site cation acetates were carried out under inert atmospheres and samples were repeatedly ground, but attempts were always met with incomplete reactions, evidenced by the appearance of significant precursor phases in XRD patterns.

3.1 Postheat treatment optimization

XRD patterns of as-synthesized samples of $A_xB_{1-x}V_2O_4$ after MW-ST synthesis exhibited broad XRD patterns indicating amorphous character and lacking well-defined peaks required for physical measurements.

At a temperature above 500°C, samples containing Co destabilized, forming a secondary phase of Co metal and V_2O_3. At a temperature above 640°C, samples containing Fe formed a Fe metal phase and a V_2O_3 phase. The remaining three samples that did not contain either Co or Fe, were MgV_2O_4, ZnV_2O_4, and MnV_2O_4.

Samples of MgV_2O_4 and ZnV_2O_4 could be fired at a temperature up to 675°, beyond which decomposition occurred. Similarly, samples of MnV_2O_4 could be annealed up to temperatures of 725°C without decomposition of the primary phase. For each sample, the first secondary phases to form were V_2O_3 and reduced Mg, Co, Zn, Fe, or Mn metals. These temperatures are a measure of the reducing strength required to destabilize each $A_xB_{1-x}V_2O_4$ sample.

3.2 Rietveld refinement of XRD patterns

Rietveld refinement was performed on each of our samples to determine whether any systematic change of the lattice size was taking place. AV_2O_4 has a cubic structure with space group (227) corresponding to $Fd\bar{3}m$ symmetry. A comparison of lattice parameters from the ICDD database are given for samples A = Mg, Co, Zn, Fe, Mn in table 2. These accepted lattice parameters also serve as the basis for the Rietveld-refined lattice parameters.

From the table of refined lattice parameters, we can see that samples do not vary significantly from the expected values. If we look at each system separately, we see that the lattice parameter does not vary monotonically for systems whose A-site cation radii are nearly similar. In contrast, for systems whose A-site cations radii differ significantly, the change in the lattice parameter is systematic as expected. This is not surprising, as similar deviations from expected values across all samples would account for this. For the Mg-Co system, the difference between Mg and Co radii in

A_x	B_{1-x}	a_R (Å)	a (Å)
Mg		8.39501(2)	8.3940
$Mg_{0.75}$	$Co_{0.25}$	8.38199(17)	
$Mg_{0.5}$	$Co_{0.5}$	8.39447(16)	
$Mg_{0.25}$	$Co_{0.75}$	8.38998(14)	
Co		8.384083(14)	8.3820
$Co_{0.75}$	$Zn_{0.25}$	8.39016(9)	
$Co_{0.5}$	$Zn_{0.5}$	8.38170(13)	
$Co_{0.25}$	$Zn_{0.75}$	8.39081(15)	
Zn		8.407816(15)	8.4028
$Zn_{0.75}$	$Fe_{0.25}$	8.409778(14)	
$Zn_{0.5}$	$Fe_{0.5}$	8.41186(4)	
$Zn_{0.25}$	$Fe_{0.75}$	8.43862(2)	
Fe		8.44549(10)	8.4530
$Fe_{0.75}$	$Mn_{0.25}$	8.45293(6)	
$Fe_{0.5}$	$Mn_{0.5}$	8.46549(6)	
$Fe_{0.25}$	$Mn_{0.75}$	8.48393(6)	
Mn		8.520534(18)	8.5200

Table 2: Lattice parameters for $A_xB_{1-x}V_2O_4$ samples. Lattice parameters measured by Rietveld refinement of x-ray diffraction patterns are given by a_R. Lattice parameters from the ICDD database are given by a and are those for which the refinement is based on and are shown for comparison.

this coordination is 0.1Å. If we interpolate linearly between the lattice parameters of MgV_2O_4 and CoV_2O_4 as an approximation for expected values of lattice paramaters for the solid solution samples, we see that deviations from these expected values are small and the lack of monotonic variation is accounted for by the small difference in A-site cation radii. Similarly, when considering the Co-Zn system, the difference between Co and Zn radii in this coordination is 0.2Å, and the lack of monotonic variation in lattice parameter can be accounted for by the small difference in radii. For the Zn-Fe system, the difference between Zn and Fe radii in this coordination is larger at 0.3Å, and accordingly, the lattice parameter varies monotonically as Zn

is replaced by Fe in this system. The difference between Fe and Mn ions in this coordination environment is also 0.3Å, and we see the same systematic variation in the lattice parameter for the Fe-Mn system as we do for the Zn-Fe system,

3.3 Magnetic properties

From the above mentioned magnetic data, a plot of inverse susceptibility was used to determine the Curie-Weiss or Néel temperature by extrapolating from the high temperature regime over which the susceptibility varies linearly. If the temperature dependence in this regime corresponds to paramagnetic behavior, then the Curie-Weiss temperature calculated from this is meaningful. However, in cases where the susceptibility behavior is not paramagnetic, the Curie-Weiss temperature calculated in this way does not reflect the correct magnetic transition temperature.

Before we analyze the susceptibility data, let us briefly revisit Curie-Weiss behavior. When a sample obeys the Curie law, the effective magnetic moment is given by

$$\mu_{eff} = \sqrt{\frac{3k_B}{N\mu_B}}\sqrt{T\chi}$$

where k_B is the Boltzmann constant, N is the Avagadro number, μ_B is the Bohr magneton, T is temperature, and χ is magnetic susceptibility. From this relationship,

we can arrive at the Curie law which is a statement of the behavior of susceptibility as a function of temperature given by

$$\chi = \frac{C}{T - T_C} \qquad \text{for} \qquad T \gg T_C$$

$$C = \frac{Ng^2 S(S+1)\mu_B^2}{3k_B} \qquad \text{(spin-only contribution)}$$

where g is the Landé g factor and S is the spin quantum number, and C is the Curie constant. With the above defined Curie constant, we can recast the Curie law as a linear relationship between inverse susceptibility and temperature.

$$\frac{1}{\chi} = \frac{1}{C}\Big(T - T_C\Big)$$

The Curie law and Curie-Weiss behavior is thereby defined by a temperature regime over which the inverse susceptibility is linear. We can employ this to determine the Curie temperature of samples. However, many of the samples do not exhibit Curie-Weiss behavior and produce spurious Curie temperatures.

Figures 4, 5, 6, and 7 show the inverse susceptibility as a function of temperature.

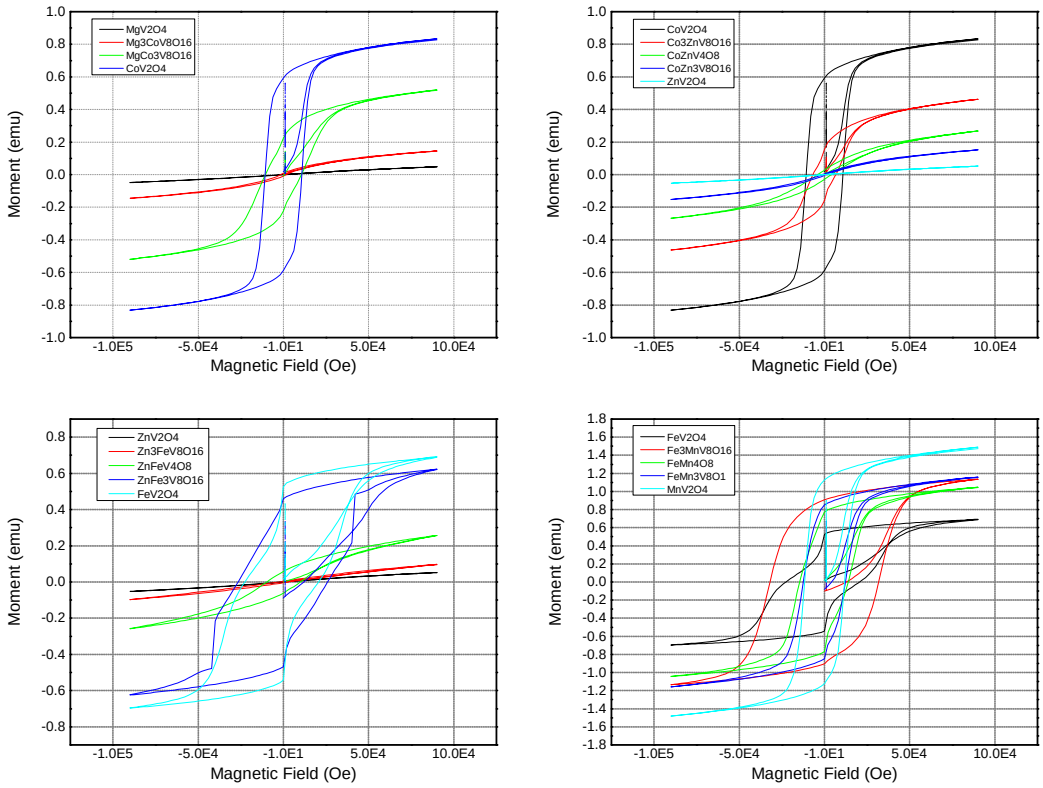

Figure 3: Magnetic hysteresis loop for a.) Mg-Co system, b.) Co-Zn system, c.) Zn-Fe system, and d.) Fe-Mn system.

From these plots, we can extrapolate the Curie-Weiss temperatures for each sample that exhibits Curie-Weiss behavior.

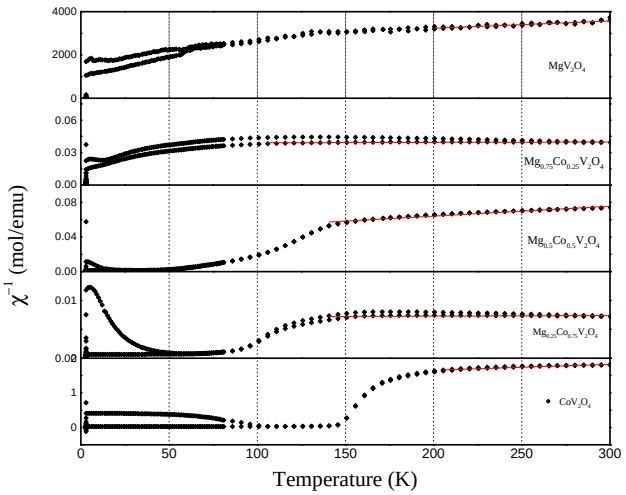

Figure 4: Inverse susceptibility of Mg-Co system. CoV_2O_4 exhibits ferrimagnetic behavior and MgV_2O_4 exhibits spurious magnetic behavior.

From this data, we can infer a Curie constant from the high temperature regime and calculate the corresponding Curie-Weiss temperature. In table 3, we can see that the transition temperature calculated this way does not, for many samples, correspond to a true magnetic transition temperature. For example, the Curie-Weiss temperature for MgV_2O_4 calculated with this method gives us a Néel temperature of $T_N = 774.4K$. Though this is much larger in magnitude than the expected magnetic transition temperature of $65K$, it is consistent with the Curie-Weiss temperature found elsewhere, and leads to a large frustration parameter, $f = 11.9$. [5], [2]

Curie-Weiss temperatures calculated this way for the Mg-Co system, and in particular for $Mg_{0.75}Co_{0.25}V_2O_4$ and $Mg_{0.25}Co_{0.75}V_2O_4$, yield very large and seemingly

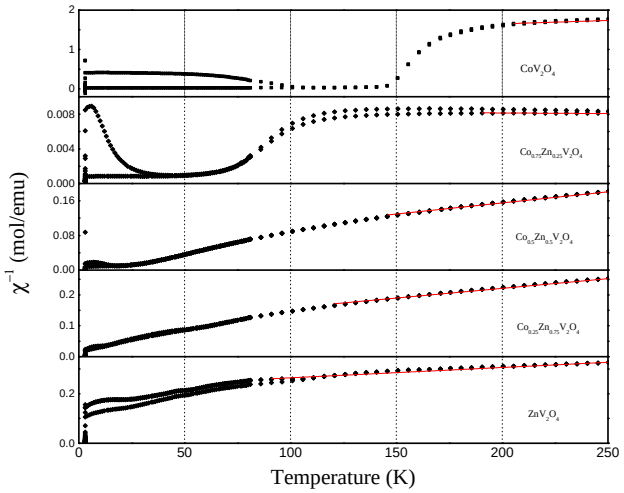

Figure 5: Inverse susceptibility of Co-Zn system. The shape of the susceptibility curve varies systematically from the ferrimagnetic behavior of CoV_2O_4 to the that of ZnV_2O_4

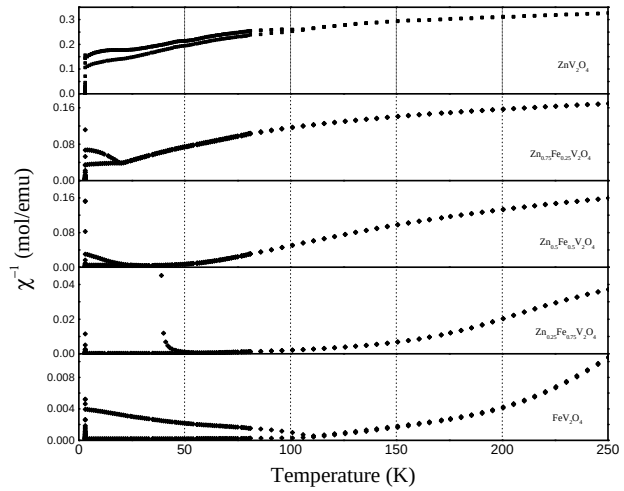

Figure 6: Inverse susceptibility of Zn-Fe system.

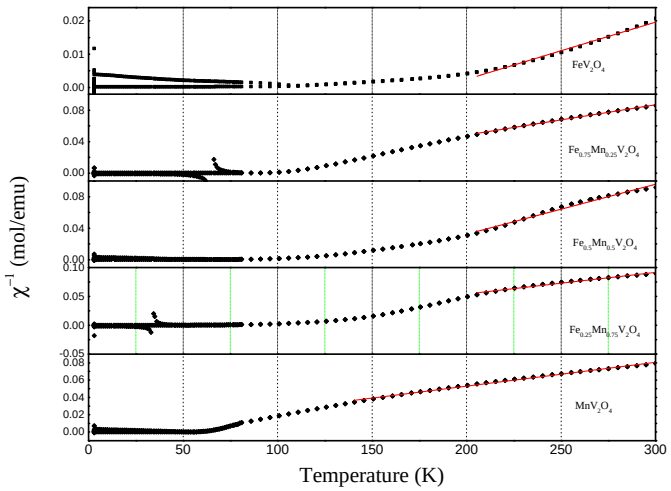

Figure 7: Inverse susceptibility of Fe-Mn system.

erroneous values and if we look at figure 4, we see that the inverse susceptibility in the high temperature region behaves in an almost temperature-independent way. This leads us to conclude that an independent method must be employed to determine the magnetic transition temperature for these samples.

While the Curie-Weiss temperature calculated in this way cannot be used directly to extract the physical magnetic transition temperature from the paramagnetic phase to a lower temperature magnetic behavior, if the diamagnetic correction is known it can be used to calculate the frustration parameter.

The Zn-Fe system and the Fe-Mn system both exhibit nearly systematic variation of the Curie-Weiss temperature.

A_x	B_{1-x}	θ_{CW} (K)	T_N (K)
Mg		-774.4	42
$Mg_{0.75}$	$Co_{0.25}$	-11189.7	
$Mg_{0.5}$	$Co_{0.5}$	-358.1	
$Mg_{0.25}$	$Co_{0.75}$	-6763	
Co		-766.7	152
$Co_{0.75}$	$Zn_{0.25}$	5804.7	
$Co_{0.5}$	$Zn_{0.5}$	-102.5	
$Co_{0.25}$	$Zn_{0.75}$	-151.8	
Zn		-533.6	40
$Zn_{0.75}$	$Fe_{0.25}$	-348.9	
$Zn_{0.5}$	$Fe_{0.5}$	-31.4	
$Zn_{0.25}$	$Fe_{0.75}$	130.5	
Fe		108	70
$Fe_{0.75}$	$Mn_{0.25}$	74.3	
$Fe_{0.5}$	$Mn_{0.5}$	149	
$Fe_{0.25}$	$Mn_{0.75}$	55.5	
Mn		7.6	156

Table 3: The Néel temperature is given for samples with a single A-site cation, as found in the literature. [7]

4 Conclusion

We have demonstrated the novel synthesis of A_x B_{1-x} V_2 O_4 solid solution samples, where A, B = Mg, Co, Zn, Fe, Mn, and x = $0, 0.25, 0.5, 0.75, 1$, using a microwave-assisted solvothermal process. A post-heat treatment was applied to each sample and the temperature of this calcination process was systematically varied to determine the temperature at which the sample decomposed into multiple phases. The seventeen samples were characterized by XRD patterns and ICP elemental analysis to determine phase information and chemical composition. Magnetic measurements of these samples were taken to calculate the Curie-Weiss temperature of each sample where appropriate.

Rietveld refinement confirmed that lattice parameter values were in agreement, up to small deviations, from expected values. For the systems Zn-Fe and Fe-Mn, where the difference in A-site cation size was large enough, the variation in lattice parameter was monotonic, as the A-site cation was replaced with a second A-site cation. This systematic change was as expected, and along with ICP results, confirmed the successful substitution of A-site cations in the A_x B_{1-x} V_2 O_4 solid solution system.

Magnetic data collected from VSM measurements showed that the Curie-Weiss temperature as calculated in details above exhibited variation within the Zn-Fe and Fe-Mn systems that was nearly sytematic. Samples for which the calculated Curie-Weiss temperature was large in magnitude and did not coincide with the physical magnetic transition temperature demonstrated large frustration parameters. Accord-

ing to XRD data, this method can successfully produce single phase A_x B_{1-x} V_2 O_4 samples, however the magnetic susceptibility data does not reflect what a Curie-Weiss law that is expected from single phase samples. Small minority phases of transition metals that were created during the synthesis or annealing process and that do not appear in XRD patterns could account for these deviations from Curie-Weiss behavior.

This work has set the stage for further work to investigate the localized-to-itinerant electron transition.

References

[1] S-H Baek, K-Y Choi, A P Reyes, P L Kuhns, N J Curro, V Ramanchandran, N S Dalal, H D Zhou, and C R Wiebe. AC susceptibility and 51 V NMR study of MnV_2O_4. *Journal of Physics: Condensed Matter*, 20(13):135218, 2008.

[2] S. Blanco-Canosa, F. Rivadulla, V. Pardo, D. Baldomir, J.-S. Zhou, M. García-Hernández, M. A. López-Quintela, J. Rivas, and J. B. Goodenough. Enhanced Pressure Dependence of Magnetic Exchange in $A^{2+}[V_2]O_4$ Spinels Approaching the Itinerant Electron Limit. *Phys. Rev. Lett.*, 99:187201, Nov 2007.

[3] S.G. Ebbinghaus, J. Hanss, M. Klemm, and S. Horn. Crystal structure and magnetic properties of ZnV_2O_4. *Journal of Alloys and Compounds*, 370(12):75 – 79, 2004.

[4] Arturo Gutierrez and Arumugam Manthiram. Microwave-Assisted Solvothermal Synthesis of Spinel AV_2O_4 (M = Mg, Mn, Fe, and Co). *Inorganic Chemistry*, 53(16):8570–8576, 2014. PMID: 25100260.

[5] Shigeo Hara, Hiroyuki Oshima, Takahiro Mastuda, Norio Umeyama, Shin-Ichi Ikeda, Miwako Takahashi, Tadataka Watanabe, and Keisuke Tomiyasu. Magnetism of the Single Crystal Mg-V-O Spinel. *Journal of Physics: Conference Series*, 320(1):012053, 2011.

[6] Yuanjie Huang, Zhaorong Yang, and Yuheng Zhang. Magnetic, structural, and thermal properties of CoV_2O_4. *Journal of Physics: Condensed Matter*, 24(5):056003, 2012.

[7] Ramandeep Kaur, Tulika Maitra, and Tashi Nautiyal. The nature of itineracy in cov 2 o 4 : a first-principles study. *Journal of Physics: Condensed Matter*, 26(4):045505, 2014.

[8] Kazuhiko Kawakami, Yoshio Sakai, and Nobuo Tsuda. Metal-Insulator Transition in $Li_xZn_{1-x}V_2O_4$. *Journal of the Physical Society of Japan*, 55(9):3174–3180, 1986.

[9] A. Kismarahardja, J. S. Brooks, A. Kiswandhi, K. Matsubayashi, R. Yamanaka, Y. Uwatoko, J. Whalen, T. Siegrist, and H. D. Zhou. $Co[V_2]O_4$: A Spinel Ap-

proaching the Itinerant Electron Limit. *Physical Review Letters*, 106(5):056602, February 2011.

[10] A. Kismarahardja, J. S. Brooks, H. D Zhou, E. S. Choi, K. Matsubayashi, and Y. Uwatoko. Dielectric properties of single crystal spinels in the series FeV_2O_4, MnV_2O_4, and CoV_2O_4 in high magnetic fields. *Phys. Rev. B*, 87:054432, Feb 2013.

[11] A. Manthiram and J. B. Goodenough. Refinement of the critical VV separation for spontaneous magnetism in oxides. *Canadian Journal of Physics*, 65(10):1309–1317, 1987.

[12] Zachary Moorhead-Rosenberg, Katharine L. Harrison, Travis Turner, and Arumugam Manthiram. A Rapid Microwave-Assisted Solvothermal Approach to Lower-Valent Transition Metal Oxides. *Inorganic Chemistry*, 52(22):13087–13093, 2013.

[13] D. B. Rogers, J. B. Goodenough, and A. Wold. Electrical Conductivity in the Spinel System $Co_{1x}Li_xV_2O_4$. *Journal of Applied Physics*, 35(3):1069–1070, 1964.

[14] R. D. Shannon. Revised effective ionic radii and systematic studies of interatomic distances in halides and chalcogenides. *Acta Crystallographica Section A*, 32(5):751–767, Sep 1976.

[15] A. Vadivel Murugan, T. Muraliganth, and A. Manthiram. One-Pot Microwave-Hydrothermal Synthesis and Characterization of Carbon-Coated $LiMPO_4$ (M=Mn , Fe, and Co) Cathodes. *Journal of The Electrochemical Society*, 156(2):A79–A83, 2009.